Improving groundwater storage change estimates using time-lapse gravimetry with Gravi4GW

Landon J. S. Halloran*†

2021-06-30

Abstract

Time-lapse gravimetry is a powerful tool for monitoring temporal mass distribution variations, including seasonal and long-term groundwater storage changes (GWSC). This geophysical method for measuring changes in gravity (Δg) is applicable to any groundwater system, but is likely to be of particular interest for studies of alpine catchments. These important catchments are highly sensitive to climate variations and can experience significant GWSC, while often lacking groundwater monitoring infrastructure. Here, we present *Gravi4GW*, a *python* tool for the calculation of β, the conversion factor between Δg and GWSC, that are site-adapted. To illustrate its usage, we investigate a detailed example of an alpine catchment and examine spatial variations and the effects of depth assumptions. This accessible tool is designed to be useful in both the planning and data-processing stages of time-lapse gravimetric field studies.

Keywords: *hydrogeophysics; gravimetry; time-lapse gravimetry; groundwater storage; alpine hydrology; numerical modelling; digital elevation model; seasonal variations*

Highlights

- Gravi4GW converts between Δg and groundwater storage changes

*Centre d'hydrogéologie et de géothermie (CHYN), Université de Neuchâtel, rue Émile-Argand 11, 2000 Neuchâtel, Switzerland.

†landon.halloran@unine.ch

- Conversion factor β can be used to target field measurements
- Use of Gravi4GW in an alpine catchment demonstrated
- The *python* software tool can use DEM or groundwater elevation data
- Effects of topography and slope on β investigated

1 Introduction

Change in groundwater storage is often the largest source of uncertainty in catchment-scale hydrological models. On the sub-catchment scale, spatial and temporal variations are difficult to constrain in the absence of direct piezometric measurements. Addressing these issues directly by drilling multiple piezometers or bores throughout a catchment involves significant financial costs and, in the case of alpine and other remote fieldsites, significant logistical challenges. Because of this, there is significant interest in non-invasive methods for measuring fluctuations in groundwater levels. Time-lapse gravimetry is a promising geophysical method that is well-suited to such investigations.

Transport of matter such as water, rock, or hydrocarbons involves a change in mass distribution which, in turn, affects the gravitational force experienced at any given point in the domain. This small change in gravity (g) can be measured at the same point in space and at two or more points in time in a technique referred to as "time-lapse gravimetry." Time-lapse gravimetry or microgravimetry measures Δg at a given point over a given time interval. This approach has been used to investigate the transport of hydrocarbons (Eiken et al., 2008; Abbasi et al., 2016; Reitz et al., 2015), sediment and rock mass (Jongmans and Garambois, 2007; Mouyen et al., 2020), and magma (Bonforte et al., 2017; Carbone et al., 2017). In hydrogeology, the technique has been used to investigate transport of groundwater on the basin (Pool and Eychaner, 1995) and field scale (Creutzfeldt et al., 2010; McClymont et al., 2012; Arnoux et al., 2020). Furthermore, the fundamental principle of time-lapse gravimetry has also been employed on a global scale in the Gravity Recovery and Climate Experiment (GRACE) (Tapley et al., 2004; Ramillien et al., 2008; Thomas et al., 2014).

Logistical, technical and financial challenges related to the installation of boreholes or piezometers are particularly salient in alpine catchments. These mountainous regions act as the world's water towers and thus a deep understanding of the hydrological state of alpine catchments is necessary (Viviroli et al., 2007; Immerzeel et al., 2020). Time-lapse gravimetry therefore has the potential to be particularly impactful in hydrological investigations in alpine catchments. The technique has already been employed to measure seasonal changes in gravity due to groundwater storage changes (GWSC) in unconfined, superficial alpine aquifers in the Canadian Rocky Mountains (McClymont et al., 2012) and in the Swiss Alps (Arnoux et al., 2020). Both of these studies employed portable gravimeters to measure gravity at multiple locations at the beginning of the post-snowmelt period and just before the onset of winter snow accumulation. Importantly, during this period, groundwater has been shown to be the major hydrological component ensuring baseflow in streams at lower elevations in alpine catchments (Clow et al., 2003; Glas et al., 2018; Hayashi, 2020). In a talus-moraine field alongside an alpine lake McClymont et al. (2012) measured predominantly negative Δg values without a discernible spatial trend, leading the authors to hypothesise that decrease in groundwater storage occurred in small pockets rather than continuously across the aquifer. In a sloping talus field above superficial moraine deposits down-gradient, Arnoux et al. (2020) found a more pronounced decrease in g in the talus which supported a conceptual model involving greater GWSC in the higher-permeability talus than in the lower-elevation moraine. In both of these studies, the authors recognised that direct conversion of Δg measurements to GWSC was not possible due to the non-uniformity of the groundwater topography, with Arnoux et al. (2020) suggesting that a numerical model would be required to provide accurate estimates of groundwater level changes.

The difficulty in obtaining quantitative estimates of GWSC from gravity measurements at the field scale has been recognised by several groups (e.g., Creutzfeldt et al., 2008; Jacob et al., 2009). Creutzfeldt et al. (2010) noted explicitly that topography determines the hydrological mass distribution and directly influences the relationship between Δg and GWSC. Some authors have used the groundwater version of the *Bouguer* plate approximation (BPA), which assumes a flat and infinite plane, to convert between Δg and GWSC (e.g. Pool and Eychaner, 1995; Jacob et al., 2009). To improve upon the BPA assumption for this conversion, Creutzfeldt et al. (2008) calculated the topography-informed conversion factor at the Wettzell Geodetic Observatory in Germany and found it to differ by $\sim$24% from that of the BPA. A subsequent study integrated continuous absolute gravity measurements into a hydrological model as a calibrating dataset (Creutzfeldt et al., 2010). El-Diasty (2016) used repeat surveys to estimate yearly GWSC in a lowland moraine aquifer in Ontario, Canada. While promising modelling studies have been performed to facilitate conversion between Δg and GWSC, they have remained site-specific. There is thus a need for a general tool to supply accurate Δg-GWSC conversion factors. This need is heightened at sites with significant topographical relief and slope, such as alpine areas, where the divergence from the BPA will be greatest.

Here, we present a novel *python* software tool for the estimation of GWSC from time-lapse gravimetry measurements. This improves on the *Bouguer* plate approximation and provides a more accurate translation between gravitational measurements and GWSC. It requires only limited input from the user and should be of interest – in both the planning and data-processing stages – for any site with non-planar topography such as that characteristic of alpine catchments where time-lapse gravimetry is particularly advantageous.

2 Theory and technical considerations

2.1. Gravity and groundwater

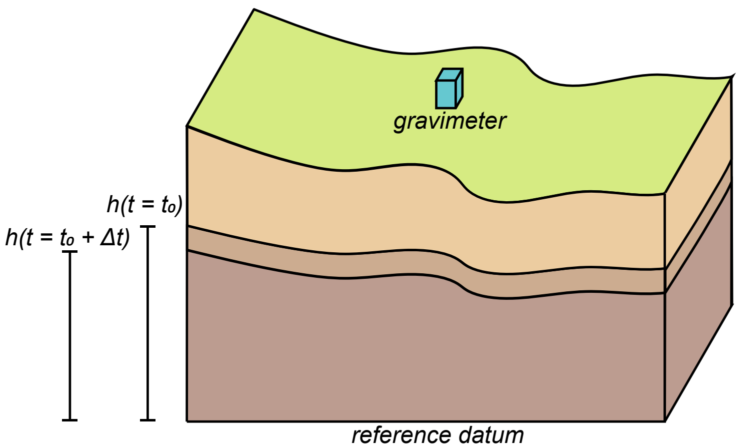

Figure 1: Simplified schematic illustrating the principle of time-lapse gravimetry. Measurements of gravity are made at the same location at times t_0 and $t_0 + \Delta t$. Here, the change in mass per area due to GWSC is $(h(t_0 + \Delta t) - h(t_0))\, \epsilon \rho_{H_2O}$ where ϵ is the porosity of the medium and ρ_{H_2O} is the density of water. This change in mass distribution will, in turn, affect gravitational force experienced at the location of the gravimeter.

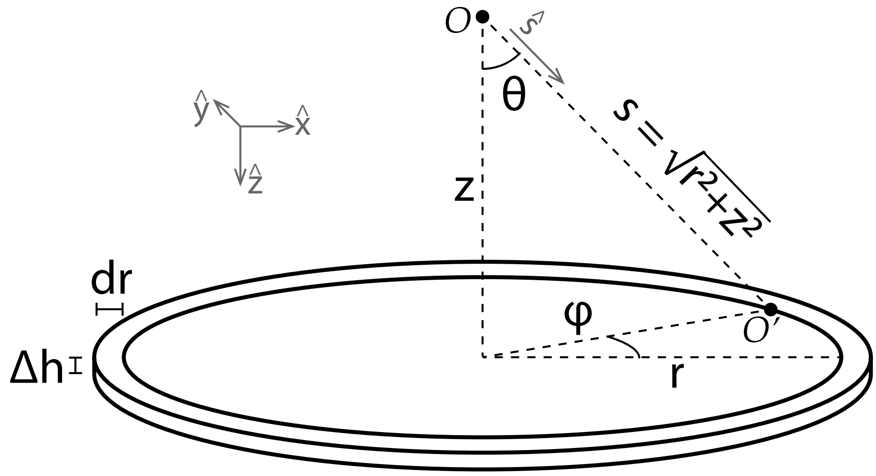

Figure 2: Coordinate definitions for evaluation of gravitational changes at point O due to a thin layer of thickness Δh.

The study of gravity has a millenia-long history and has been central to our understanding of the universe. For the purposes of time-lapse gravimetry for geosciences, Newton's 17th-century theory is, fortunately, sufficient and later relativistic developments by Einstein and others can be safely ignored. Here we use the standard definition of g, the measurable quantity of gravity, as the gravitational force F_g per mass m experienced by an object of mass m. The value of g varies between approximately 9.78 and 9.83 m/s^2 across the surface of the Earth. Its value is affected by all matter can be formulated as:

$$\vec{g} = G \iiint \frac{\rho(\vec{s})}{s^2} \hat{s} d^3x \tag{1}$$

where G is the universal gravitational constant (6.674 $\times$ 10^{-11} m^3 kg^{-1} s^{-2}), $\rho(\vec{s})$ the mass density at point $\vec{s}$. For groundwater time-lapse gravimetry, the underlying assumption is that either the only local change in mass distribution is due to the movement of water or that any other mass distribution changes have been accounted for. Thus, by measuring g at the same location at two (or more) points in time, the change in mass distribution over the period is indirectly measured (Figure 1). Following Equation 1, the change in gravity at a given point due to a change in mass distribution $\Delta\rho(\vec{s})$ can be defined as:

$$\Delta\vec{g} = G \iiint \frac{\Delta\rho(\vec{s})}{s^2}\hat{s}d^3x \tag{2}$$

We define $\vec{\beta}$ as the rate of change in gravity as the water table decreases by a unit height (i.e., the effective height of an equivalent free water column):

$$\vec{\beta} = \frac{\partial\vec{g}}{\partial h} \tag{3}$$

Where β is written without the vector arrow, we refer to the absolute value of $\vec{\beta}$, i.e.:

$$\beta = |\vec{\beta}| \tag{4}$$

Correspondingly, β_z is defined as the vertical component of the gravity change and β_r as the radial component:

$$\beta_z = \frac{\partial\vec{g}}{\partial h} \cdot \hat{z} \tag{5}$$

$$\beta_r = \left[\left(\frac{\partial\vec{g}}{\partial h} \cdot \hat{x}\right)^2 + \left(\frac{\partial\vec{g}}{\partial h} \cdot \hat{y}\right)^2\right]^{\frac{1}{2}} \tag{6}$$

To measure the degree to which changes in gravity due to GWSC vary from vertical, we can also define (following the coordinate system definitions of Figure 2):

$$\theta_\beta = \arccos\left(\frac{\beta_z}{\beta}\right) = \arcsin\left(\frac{\beta_r}{\beta}\right) \tag{7}$$

To illustrate the principle and to make first-order estimates of error introduced by finite integral ranges, we simplify calculations here to planar water table topography using the coordinate system as defined in Figure 2. The change in gravity at point O due to an infinitesimal change in the water table height of Δh gives:

$$\Delta\vec{g} = (\Delta h)G \iint \frac{\hat{s}dm}{|\vec{s}|^2} \tag{8}$$

where $\hat{s}$ is a unit vector in the direction of integration point O'. We note that if, due to symmetry, changes in groundwater storage influence only the vertical component, $\beta_z = \beta$ and $\theta_\beta = 0$. As the thickness of the plane is decreased,

$$\beta = G \iiint \frac{\hat{s} \cdot \hat{z}}{|\vec{s}|^2} dm \tag{9}$$

Assuming uniform density ρ, we obtain:

$$\beta = G\rho \iint \frac{r \cos\theta}{|s|^2} d\phi dr \tag{10}$$

Taking advantage of radial symmetry and integrating up to a radial distance of r_0, we obtain:

$$\beta = 2\pi G\rho \int_0^{r_0} \frac{rz}{(r^2 + z^2)^{3/2}} dr = 2\pi G\rho \left[1 - \frac{1}{\sqrt{1 + (\frac{r_0}{z})^2}}\right] \tag{11}$$

As has been remarked by several (e.g. Leirião et al., 2009; Arnoux et al., 2020), for water of density 1000 kg/m^3, when $r_0 \to \infty$, this evaluates to β = 4.193 $\times$ 10^{-7} s^{-2} or 41.93 μGal/m$_{H_2O}$. Expressed otherwise, under the infinite plane assumption, a GWSC of $\sim$2.38 cm will lead to a change in vertical gravity of 1 μGal or 1$\times$10^{-8} m/s^2. This is the groundwater *Bouguer* plate approximation (BPA). Importantly, this derivation enables estimation of the error in β imparted by evaluating to a finite radial distance r_0, as is necessary in a numerical implementation:

$$\epsilon = \frac{1}{\sqrt{1 + (\frac{r_0}{z})^2}} \approx \frac{z}{r_0} \tag{12}$$

where the approximation is valid for $r_0 >> z$. This mirrors the remarks of Leirião et al. (2009) who described the gravitational "footprint" of GWSC as 10 times the depth to the water table beneath the measurement location, which corresponds to $\sim$90% of the change in gravity. This approximation is used in the *Gravi4GW* software presented here to determine the numerical integration domain as a function of defined acceptable error subject to data availability.

This conversion factor β can be expressed in units of s^{-2} or μGal/m. As the calculation is made in terms of gravitational change per unit of equivalent free water column, we can also write

μGal/m$_{H_2O}$ to be explicit. Conversions between changes in water table elevation and changes in equivalent free water column can be made by considering porosity.

2.2. Gravimeters and gravimetric surveys

Gravimeters measure the amplitude of the gravitational field at their measurement location, with precision in the μGal (10^{-8} m/s^2) range currently achievable. Both absolute and relative gravimeters exist. The general operating mechanism of many gravimeters is a suspended mass attached to a spring in a vacuum. The weight of the mass changes as a function of gravity, which, in turn, affects the length and force on the spring which can be measured by means of optical or electronic amplification. Other mechanisms for gravity measurement, including quantum effects and wave interferometry, also exist, although these generally involve supercooling (e.g., Boy and Hinderer, 2006; Bidel et al., 2018). Absolute gravimeters such as the μQuans Absolute Quantum Gravimeter or Micro-g LaCoste A10 provide absolute measurements of g. These are generally suited to stationary measurement at a fixed location where they measure near-continuous temporal variations in gravity or require transport by vehicle which makes them non-ideal for carrying out measurements at multiple field locations over the course of a single day. Measurements made with absolute gravimeters will nonetheless benefit from the approach detailed in this work if the target application is GWSC.

Relative gravimeters such as the Scintrex CG-5 and CG-6 (Scintrex, 2018) provide a relative measurement of gravity are suited to field applications, even in rugged terrain, as they can be readily transported from one location to another by a single person on foot. They require repeated measurements at a fixed location throughout each survey to enable drift correction, as well as a reference measurement. For true quantification of GWSC, the reference measurement or measurements are made at an absolute gravity station in each survey.

For time-lapse gravimetry, the location of the gravimeter at repeat measurements must be well-constrained – in particular, vertically – through corrections for small elevation differences between surveys. A 1 cm error in elevation equates to a ~3.1 μGal error in gravity (Seibert and Brady, 2003; Arnoux et al., 2020), which is within the range of accuracy offered by portable gravimeters.

As sub-centimetre accuracy and precision is available in modern GNSS surveying systems, they should thus be considered a necessity for any time-lapse gravimetry campaign.

A final correction to gravimetry data is that related to Earth tides. Earth tides are known, periodic variations in gravity due to the changing relative positions and orientations of the Earth, Sun and Moon, as well as, to a much lesser extent, other celestial bodies. These variations in gravity are generally <100 μGal in amplitude and their impact on groundwater pressures can be exploited to estimate hydro-physical properties of aquifers (Cutillo and Bredehoeft, 2011; Acworth et al., 2016; Rau et al., 2018). For time-lapse gravimetry, Earth tides must be accounted for over the course of a single survey, as well as across repeat surveys. Some gravimeters implement the Longman (1959) formulae and can perform internal corrections; however, the current state-of-the-art is ETERNA (Wenzel, 1996; Kudryavtsev, 2004) and its *python* implementation pyGtide (Rau, 2018). Significant differences between these and the Longman (1959) formulae have been noted (Arnoux et al., 2020). Thus, due to the precision required in estimating GWSC, it is recommended that these corrections are made in the most accurate and precise manner possible.

3 Software

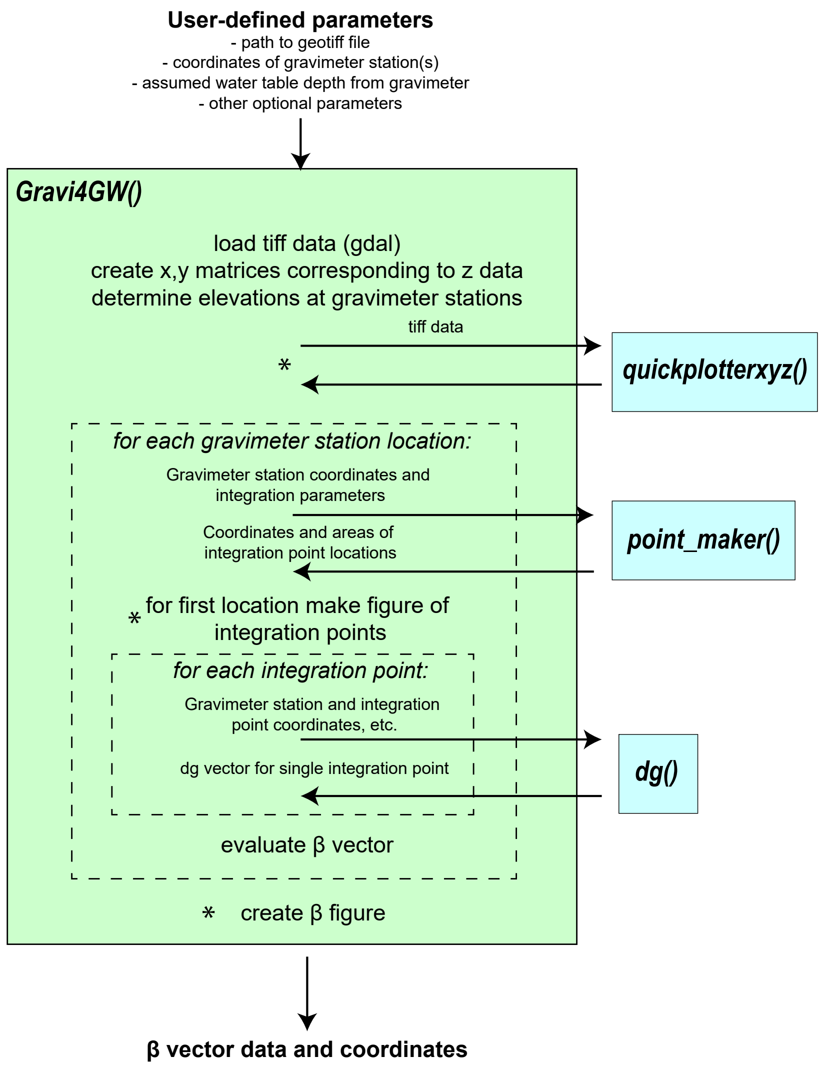

Figure 3: Simplified schematic of the program flow of Gravi4GW. Asterisks (*) denote optional plotting tasks and dashed boxes denote loops.

Gravi4GW implements the calculation of $\vec{\beta}$ (Equation 4) based on user-provided data. This data includes a digital elevation model or water table model and locations of gravity stations. The program can be supplied the coordinates of a single gravimetry station or a grid of multiple gravimetry stations which enables the creation of a map of β. Additional plotting facilities for the input data and for the numerical integral are also included. Figure 3 shows the basic process flow of the software. The program can be executed with a single line of *python* code, although some short preamble code is required to define the input data.

The software is written in the *python* language, which is reputed for its clean, readable syntax that should facilitate modifications by end-users. The dependencies of *Gravi4GW*; *numpy* (Harris et al., 2020), *matplotlib* (Hunter, 2007), *scipy* (Virtanen et al., 2020), and *gdal* (GDAL/OGR Contributors, 2020); are well-maintained and extensively-documented standard packages. The software makes use of the *gdal* framework to read input files of *geotiff* format. These files may contain data from digital elevation models (DEMs) or groundwater elevation models. A meter-based coordinate reference system (CRS) is assumed and thus data using other types of CRS (e.g., longitude-latitude in degrees) must be converted prior to use with `Gravi4GW`. Further information regarding program inputs is contained in the software documentation.

Several utility functions are integrated into the software. The most important of these are *pointmaker* and *dg*. Additionally, a simple plot of the input file and created x and y coordinate matrices is optionally outputted using the *quickplotterxyz* function. The *pointmaker* function creates a mesh grid for numerical integration of Equation 2. It is called once for each gravimetry station and operates using radial coordinates centred at the station before converting to the cartesian coordinate system of the input data. Inputs for the function include parameters controlling radial extent and radial and azimuthal point density. The radial coordinate point density follows a logarithmic distribution and the maximum radius is defined based on a user-defined acceptable error criterion (Equation 12). The function also returns the representative area for each point. The gravity integral is evaluated using the *dg* function, which is called once for each integration mesh point created by *pointmaker*. For each of these points, the gravity vector,

$$\Delta\vec{g} = \Delta g_x \hat{x} + \Delta g_y \hat{y} + \Delta g_z \hat{z} \tag{13}$$

is evaluated in Cartesian coordinates (see Figure 2):

$$\Delta g_x = (\Delta g)\cos(\theta)\sin(\phi) \tag{14a}$$

$$\Delta g_y = (\Delta g)\cos(\theta)\cos(\phi) \tag{14b}$$

$$\Delta g_z = (\Delta g)\sin(\theta) \tag{14c}$$

where Δg is calculated following Equation 2. A sufficiently small value (1 cm) is used for Δh to evaluate the $\vec{\beta}$ vector (Equation 4).

In terms of execution time, we provide indicative times using *python* 3.7.6 in *Anaconda Spyder* 3.3.6 on a Windows 10 laptop with 16GB of ram and i7-7600U 2.8 GHz processor. Using 2 m resolution input data and 1257 integration mesh points, corresponding to a maximum integration radius of 500 m with 40 points radially, *Gravi4GW* takes $\sim$1.8 s to evaluate $\vec{\beta}$ at a single gravity station point without plotting options and 16.3 s to evaluate it at 100 gravimetry station points with plotting options. Efficiency is gained by exploiting a regular grid and thus using the *RectBivariateSpline* class in *scipy* to estimate the elevations in the Δg numerical integral. Additional details regarding the use of *Gravi4GW* are available in the software repository *readme* file and in the program functions themselves.

4 Application

4.1. Site description

As an illustrative example, we use 2 m resolution digital elevation data from the Swiss Federal Office of Topography (Swisstopo) with an approximate centre of 7.53 °E, 46.19 °N and of pixel dimensions 4670$\times$2357. The dataset follows a regular grid and spans 2602058 to 2611396 east-west and 1113079 to 1117791 north-south in the Swiss CH1903+ (LV95) CRS. It includes part of the Vallon de Réchy (Mari et al., 2013; Cochand et al., 2019) and the entirety of the Tsalet catchment (Arnoux et al., 2020). Cochand et al. (2019) provide a thorough geological and hydrological description of the greater Vallon de Réchy in which the catchment is located. The Tsalet catchment is characterised by moraine and talus deposits and undergoes a seasonal cycle of groundwater storage (Arnoux et al., 2020). This cycle, wherein groundwater levels decrease over the period between the end of spring snowmelt and, at the earliest, the onset of winter snow accumulation, is typical of alpine catchments (Cartwright et al., 2020; Hayashi, 2020; Arnoux et al., 2021). The spatial and temporal variations in groundwater storage are of interest here primarily due to their importance in ensuring baseflow in streams down-gradient.

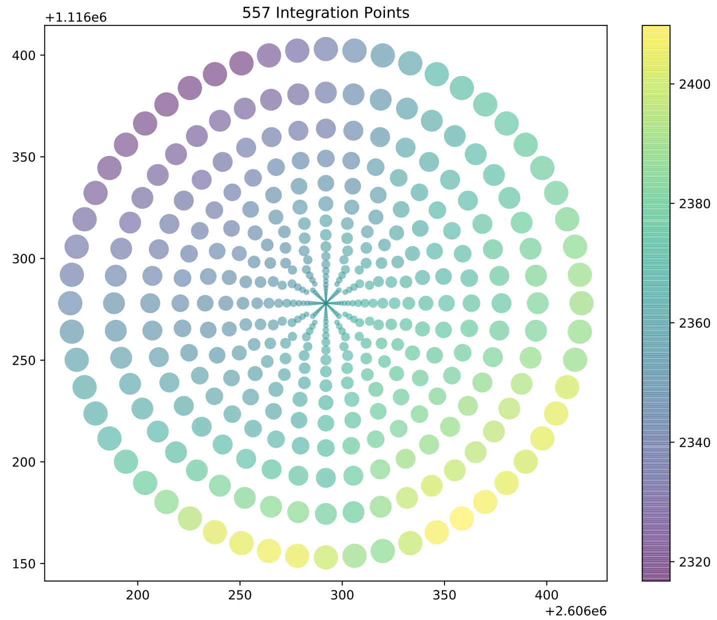

Figure 4: Visualisation of the mesh points used to evaluate the Δg integral (Equation 2). This example is the result of an assumed effective groundwater depth of 2.5 m, an acceptable residual of 2%, a radial point count of 40, and an azimuthal density setting of 8. The size of each circle corresponds to the area it represents and the colour scheme corresponds to the effective elevation of each point in meters. Figures of this type are optionally created by *Gravi4GW* following a call of *pointmaker* function (Figure 3) which defines the integration mesh.

4.2. Calculating β and its spatial variability

In order to illustrate usage of *Gravi4GW* and to investigate spatial variance and the influence of assumed effective water table depth, we generate maps of β (Equation 4) assuming depths to the effective water table of 2.5 m, 5 m and 7.5 m. Vectors of spatial locations in the same CRS as the input data, in this case a DEM, are supplied to *Gravi4GW* which then evaluates the Δg integral numerically for each location (Figure 3). The numerical integral is calculated by generating a set of point-area pairs, i.e., an integration mesh. We set an acceptable residual of 2%, therefore requiring that the integration mesh be extended to 50× the assumed effective water table depth beneath each gravimetric station, h_{eff} as per Equation 12. We also set the number of radial distances at which mesh points are to be created to 40 and use the default azimuthal density setting of 8. These settings result in 557 integration points for $h_{\text{eff}} = 2.5$ m, with the area represented by a mesh point ranging from $2.2{\times}10^{-3}$ m^2 for the points nearest to the gravimetry station location to 333 m^2 for the farthest ones (Figure 4). These values depend on the input parameters for the *pointmaker* function and can be thus controlled by the user. The density of points decreases radially, while a minimum azimuthal point density is also maintained (Figure 4). This type of integration mesh point density is suitable due to the $\propto 1/r^2$ nature of gravitational force and provides an appropriate balance between numerical efficiency and accuracy.

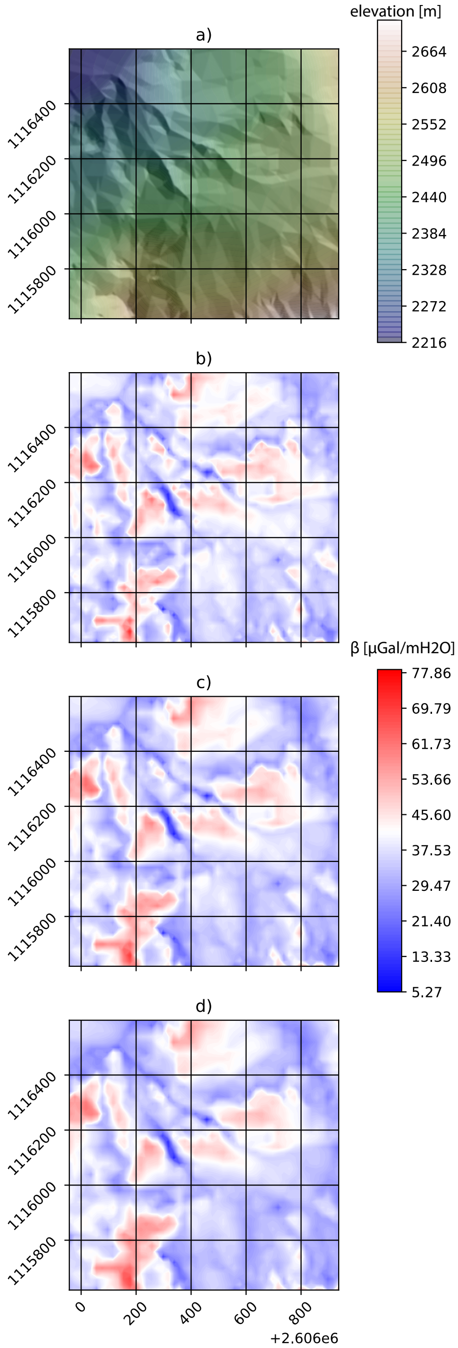

Figure 5: Maps of β (Equation 4) in units of μGal/m$_{H_2O}$ as estimated by Gravi4GW using a digital elevation model *(a)* as input. Different results are obtained in assuming different values of h_{eff}: *(a)* 2.5 m, *(c)* 5 m, and *(d)* 7.5 m. The CRS is CH1903+ (LV95).

For each of the h_{eff} values and for each gravimeter station coordinate pair, a set of mesh points is generated and $\vec{\beta}$ is evaluated in the same cartesian CRS as our input (CH1903+/LV95). This enables the creation on a β map (Figure 5). Generally, values of β are greatest in regions of convex topography (mounds, hills, ridges, etc.) and smallest in those of concave topographies (dolines, depressions, channels, etc.). This can be seen in Figure 5 where the lowest values are observed in the beds of intermittent streams and the highest values are observed on mounds. At the highly concave locations, there is likely to be the greatest divergence between topographically-informed β values and the true dependence of gravity on GWSC. As the realistically attainable measurement uncertainty for time-lapse gravimetry measurements using a portable gravimeter is likely to be in the $\sim$5 μGal range (McClymont et al., 2012; Arnoux et al., 2020), it is thus advisable that one should avoid areas of extreme concave curvature and instead targets gravity measurement locations with moderately convex or planar topography.

Spatial variations in β are most abrupt when h_{eff} is relatively shallow. This is due to the more pronounced effect of local curvature. As the assumed depth to the water table increases, the effective radius of influence or "footprint" (Leirião et al., 2009) increases as illustrated for planar topography in Equation 11 wherein 90% of the Δg signal can be attributed to the area within a radial distance of $\sim$10 times the depth to the water table below the gravimetric measurement point. Thus, with increasing h_{eff}, the influence of features in the immediate vicinity of the gravimetry station is weakened.

4.3. Dependence of β on groundwater table depth

Assumed effective groundwater depth, h_{eff}, is a necessity in calculating β, yet in practical applications it will not be known. Indeed, this presents a circuitous problem as the depth to the groundwater table and its change over time constitutes, in part, what one seeks to understand when using time-lapse gravimetry. Additionally, as the depth to the groundwater table changes, β may also change. In this way, accurate conversion between Δg and GWSC – as well as quantification of uncertainty – may require an understanding of the dependence of β on the assumed effective depth to the groundwater table when the changes in groundwater storage are significant. It is therefore useful to investigate the effect of this assumed groundwater depth parameter on β. Furthermore, the directionality of Δg is not necessarily co-directional with the gravity vector, which defines the z direction in a geodetic CRS. This will generally be the case in any sloped terrain, although the difference between β and β_z will be constrained to <5% for slopes with gradients <18° (<33% grade). *Gravi4GW* calculates the $\vec{\beta}$ vector, thus it is possible to investigate its the vertical and non-vertical components.

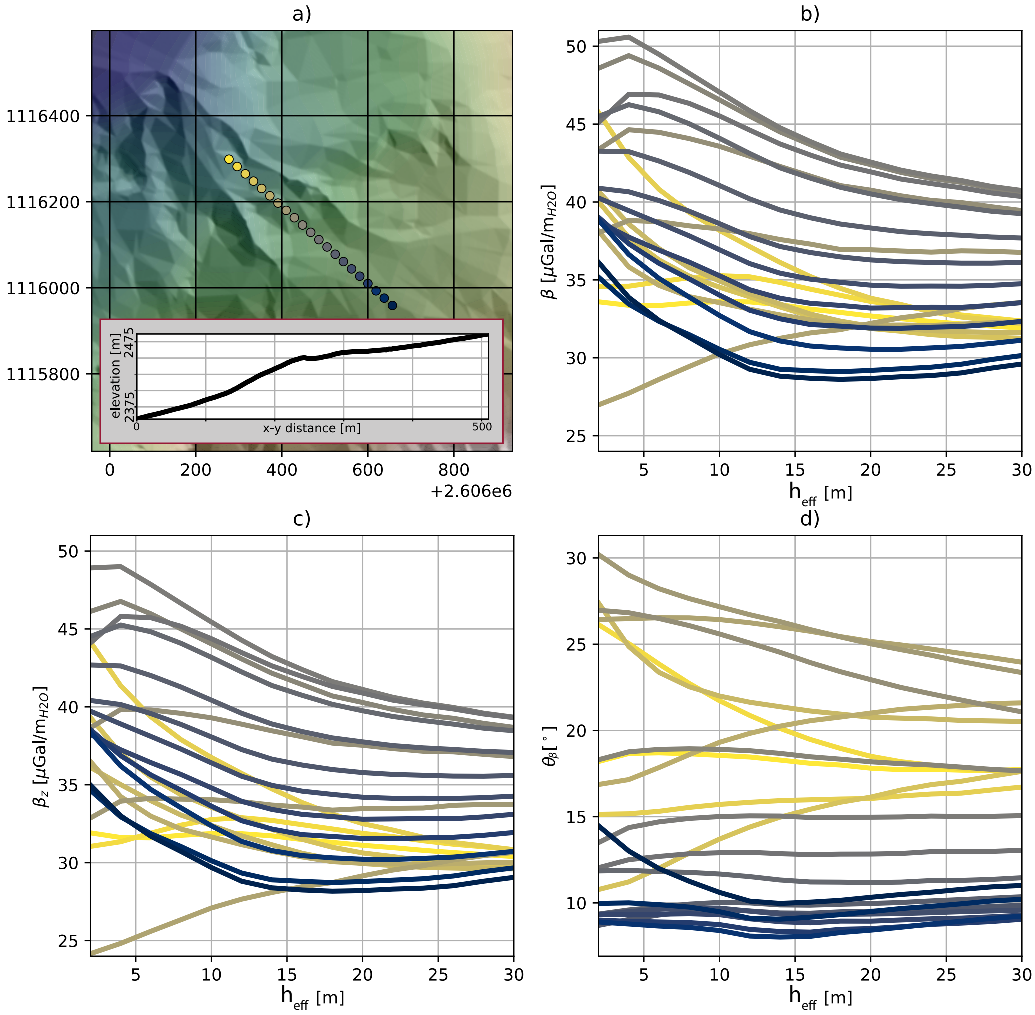

Figure 6: The variability of β, β_z, and θ_β at several locations as a function of the assumed effective depth from the gravimeter to the water table (h_{eff}). *a)* Locations at which the values are calculated. The colours of the points here correspond to those of the β, β_z, and θ_β subplots. The topographical profile along the transect is shown as an inset. The values of *b)* β (Equation 4), *c)* β_z (Equation 5), and *d)* θ_β (Equation 7) as a function of h_{eff} at these locations.

We define a series of 21 evenly-spaced points spanning 510 m horizontally, roughly aligned NW-SE (Figure 6a). This transect covers a central part of the catchment and sits between two intermittent stream channels. At each of these points we evaluate $\vec{\beta}$ at h_{eff} of 2 – 30 m and additionally calculate θ_β (Equation 7), the angle between $\vec{\beta}$ and the vertical vector $\hat{z}$ (Figure 6). The highest variability in β, both across the points and as a function of h_{eff}, occurs for small values of h_{eff}, i.e., when the assumed effective depth to the groundwater table is shallow. This is due to the greater influence of small-scale local topography at low h_{eff} values. As h_{eff} increases, so does the extent of the GWSC "footprint" affecting β. A most extreme example of this is the sixth lowest point with the lowest β value at $h_{\text{eff}} = 2$ m (Figure 6b). In contrast to the neighbouring points, this location lies at the bottom of a local depression in the direction perpendicular to the transect. As expected, this local concave topography causes the value of β to be less than that stemming from the groundwater Bouguer plate approximation (41.93 μGal/m$_{H_2O}$). However, as h_{eff} increases, this effect is dampened as the local depression represents an increasingly smaller proportion of the region of influence.

The vertical component and, consequently, the direction of the $\Delta\vec{g}$ vector also change as a function of h_{eff} (Figure 6c & d). The lower half of this transect has a steeper gradient than the upper half (Figure 6a inset). Along the transect, the lowest six points have local gradients of between 14.4° and 20.5° while the next four points have slopes between 24.9° and 29.8°. Above this, the slope along the direction of the transect is between 3.6° and 12.4°. We observe that θ_β has the greatest variance for small h_{eff}. As h_{eff} increases, the θ_β values of the upper region, where the topography is more uniform, approach values similar to the local topographical slope. In the hypothetical case of a uniform sloping plane, one would expect the orientation of the $\Delta\vec{g}$ vector to be perpendicular to the gradient; however, as topography is non-planar, θ_β does not tend exactly towards the local slope of the terrain.

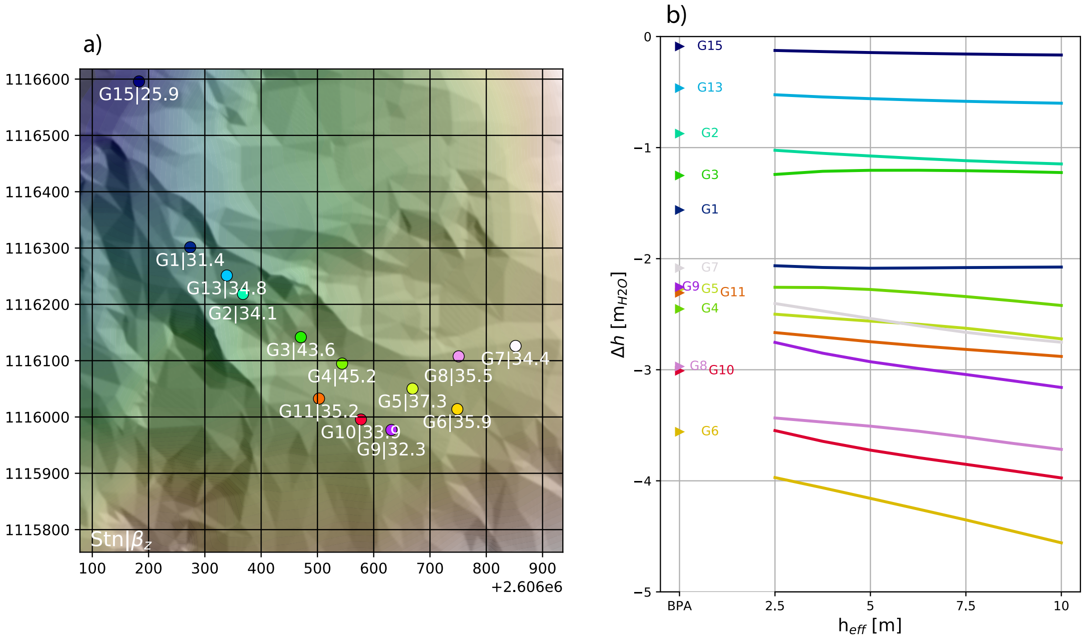

Figure 7: *a)* Time-lapse gravimetry station locations and β_z values [μGal/m$_{H_2O}$] calculated by *Gravi4GW* with a setting of $h_{\text{eff}} = 5$ m. b) GWSC inferred from time-lapse gravimetry measurements in the Tsalet catchment. The triangles display the values as calculated using $\beta_z = 41.93$ μGal/m$_{H_2O}$ (*BPA* = *Bouguer* plate approximation). The lines display the GWSC values calculated using β_z as generated by *Gravi4GW* at a range of assumed effective depths to the groundwater table. Gravimeter sensor height (0.48 m) is taken into account in the calculation. Data adapted from Arnoux et al. (2020).

4.4. Using β with time-lapse gravimetric data

Relative time-lapse gravimetry measurements were carried out in the Tsalet catchment in July and October 2019 by (Arnoux et al., 2020). These dates correspond to the end of the spring/summer snow-melt period and just prior to the onset of autumn snowfall and thus were expected to correspond to a period of significant decrease in groundwater storage. Typical of small, alpine catchments with complex topography (Cowie et al., 2017; Cochand et al., 2019; Hayashi, 2020), there are no wells or piezometers in the catchment. However, the drying of intermittent streams indicated negative GWSC. Arnoux et al. (2020) observed greater decreases in gravity in the upper talus-dominated portion of the surveyed area. The authors stated that the results could only be used to look at relative differences across different parts of the catchment due, in major part, to the likely variability of β from one gravimeter station to another. Here, we use *Gravi4GW* to make Δg to GWSC conversions using β_z (Figure 7). Additionally, we test the influence of assumed effective depth to the water table, whose precise value is unknown.

Calculated with $h_{\text{eff}} = 5$ m, the value of β_z at all but two of the thirteen time-lapse gravimetry stations is less than that of the groundwater BPA, and significant variability between locations exists. Notably, for most stations, uncertainty in h_{eff} has less of an effect on the calculated GWSC values than does the choice to use the more advanced method of *Gravi4GW* in place of the BPA. At station G1, for example, *Gravi4GW*-determined GWSC values varies between −2.06 and −2.09 m for the range of h_{eff} explored, whereas the BPA-determined value is −1.56 m. While the converted GWSC do not change the overall conclusions of greater GWSC in the upper talus area of the catchment compared to those in the lower moraine region, they do provide a means for making more quantitative interpretations.

5 Discussion

Time-lapse gravimetry is well-established as a powerful tool for the indirect measurement of changes in mass distribution over time. However, its truly quantitative use in groundwater studies has been held back by the lack of straightforward tools for conversion between Δg and GWSC. *Gravi4GW* seeks to fill this void. While gravimetry is not a direct substitute for piezometric measurements, it does provide valuable information where drilling bores or piezometers is not feasible due to logistical or financial constraints. The Tsalet catchment presented as our example application typifies an instance where time-lapse gravimentry can offer significant insight into hydrogeological processes.

When using the outlined topographically-informed conversion factors between Δg measurements and GWSC, it is useful to consider the meaning of β as compared to β_z. On sloping terrain in particular, this consideration is important as the values of these two may differ significantly. This occurs due to the directionality of the change in gravity imparted by the increase or decrease in local groundwater storage, which may be non-vertical. The precision that would be required to directly measure the directionality of this vector would be extremely fine and, indeed, most gravimeters do not measure the direction of gravity. For example, a Δg value of -100 μGal with a θ_β value of 20° would only impart a change in the direction of $\vec{g}$ of $\sim 2\times10^{-6}$ °. This means that the off-vertical components in Δg due to GWSC are not measurable. What is actually measured in time-lapse gravimetry is the vertical component of Δg, or Δg_z, and therefore the quantity calculated by *Gravi4GW* that is of greatest interest for conversion between Δg and GWSC is β_z (Equation 5).

Defining a maximum radius for the Δg integral numerical calculation is necessary. This is done via the acceptable error criterion (Equation 12) in *Gravi4GW*. Due to the r^{-2} dependence of the gravitational force, this radius need not be prohibitively large, but its finite value will nonetheless impart some error. The software does not calculate the effects on gravity beyond the user-defined radius and does not modify the β value after its calculation. Some users may nonetheless wish to normalise the resultant β values by a factor of $\frac{1}{1-\epsilon}$, which implicitly assumes that integrating to infinity would result in an increase in β. This, however, may not be strictly true if an increase in the integration radius results in the integration of mass at a higher average elevation than the gravimetry station, thus decreasing β, albeit slightly. It is thus suggested that the integration radius as defined through Equation 12 not extend to zones where groundwater response is likely to be weaker than that of the unconfined aquifer of interest. To go beyond this level of precision, the input data to *Gravi4GW* would need to be informed by a groundwater model of some sort.

Time-lapse gravimetry is likely to be most useful for investigating unconfined, shallow aquifers. Unconfined aquifers experience much greater changes in water content due to the piezometric surface being equivalent to the water level in the aquifer. They are also more likely to be the site of seasonal changes in groundwater storage due to their direct connection with the Earth's surface. As shown, where the water table is shallow, the effect of local variations in GWSC on gravity is pronounced as the groundwater gravitational "footprint" is smaller (Leirião et al., 2009). Thus the spatial resolution possible through the use of time-lapse gravimetry is greater. The piezometric surface that defines the water table will not generally be known *a priori* in a study that uses time-lapse gravimetry. Indeed, if it were known, there would be little interest in deploying geophysical methods to characterise its changes. Our results show that, despite this uncertainty in h_{eff}, there is much to be gained from the use of the approach implemented in *Gravi4GW*, especially so when the alternative is the constant BPA. In the absence of other information about the water table, *Gravi4GW* provides the user with a range of β values and hence a range of GWSC as expressed in meters of water equivalent. This is, ultimately, the quantity of interest in time-lapse gravity studies. The linear topographical influence on water table elevation that is calculated when a DEM is provided as input data can be viewed as a first-order approximation, with the true topology of the surface possibly exhibiting less curvature than the land surface. Thus, digital elevation data of lower resolution than that used as an example in this work (2 m resolution) may also provide consistent results. It follows from the earlier discussion of the effective spatial resolution of time-lapse gravimetry that the influence of local surface curvature on β will decrease as the depth to the water table increases. For a greater order of accuracy in calculating β, a groundwater elevation model (e.g., Beven and Kirkby, 1979; Thompson and Moore, 1996; Brunner and Simmons, 2012), into which additional knowledge of local hydrogeological conditions could be integrated, could be used in place of a DEM.

Finally, while we have focused primarily on the evaluation of β to estimate GWSC using time-lapse gravimetric measurements, *Gravi4GW* can also be used in the geophysical fieldwork planning phase. Maps of β such as those of Figure 5 can serve to guide researchers to locations where gravimetric measurements are likely to provide the greatest value. Locations with higher values of β (specifically, β_z) should be targeted as they are likely to yield the greatest, and thus most readily measurable, Δg values.

6 Conclusions

Gravi4GW provides a flexible tool for the calculation of groundwater storage changes based on observed changes in gravity. Integration of complimentary data into it will likely be of interest to certain users depending on the nature of their study and zone of interest. We envision the software being used in both the preparation phase and the processing phase of time-lapse gravimetry field campaigns. For preparation, DEM- or groundwater elevation model-informed β maps created by *Gravi4GW* can be used to target zones where GWSC will have the greatest gravimetric "signal". In the processing phase, *Gravi4GW* enables conversion between measured Δg and GWSC, as well as an analysis of uncertainty due to the unknown depth to the groundwater table. The tool can be executed in a single line of code by even novice *python* users. Due to its utility and simplicity of use, it is expected that *Gravi4GW* will assist hydrogeologists, geophysicists and environmental scientists in using gravimetry to make quantitative assessments and to arrive at better-informed conclusions when investigating changes in groundwater storage.

Software availability

Gravi4GW is developed by Landon Halloran (`www.ljsh.ca`) and is available at `www.github.com/lhalloran/Gravi4GW`. It is written in *python* 3.7 and requires standard packages *numpy* (Harris et al., 2020), *matplotlib* (Hunter, 2007), *scipy* (Virtanen et al., 2020), and *osgeo.gdal* (GDAL/OGR Contributors, 2020). The core *Gravi4GW.py* program is <20 kB in size, while the package with included example scripts, input data, and output is ~87 MB. It has been built and tested in the Spyder 3.3.6 IDE (`www.spyder-ide.org`) as included in the open-source *python* distribution platform *Anaconda* Individual Edition (`www.anaconda.com`).

Acknowledgements

Most figures were made using *matplotlib* (Hunter, 2007). Hillshading code was adapted from Github user Roger Veciana i Rovira (*rveciana*).

References

Abbasi, A., Annor, F., and van de Giesen, N. (2016). Investigation of Temperature Dynamics in Small and Shallow Reservoirs, Case Study: Lake Binaba, Upper East Region of Ghana. *Water*, 8(3):84, doi:10.3390/w8030084.

Acworth, R. I., Halloran, L. J., Rau, G. C., Cuthbert, M. O., and Bernardi, T. L. (2016). An objective frequency domain method for quantifying confined aquifer compressible storage using Earth and atmospheric tides. *Geophysical Research Letters*, 43(22):671–11, doi:10.1002/2016GL071328.

Arnoux, M., Brunner, P., Schaefli, B., Mott, R., Cochand, F., and Hunkeler, D. (2021). Low-flow behavior of alpine catchments with varying quaternary cover under current and future climatic conditions. *Journal of Hydrology*, page 125591, doi:10.1016/j.jhydrol.2020.125591.

Arnoux, M., Halloran, L. J. S., Berdat, E., and Hunkeler, D. (2020). Characterizing seasonal groundwater storage in alpine catchments using time-lapse gravimetry, water stable isotopes and water balance methods. *Hydrological Processes*, 34(22):4319–4333, doi:10.1002/hyp.13884.

Beven, K. J. and Kirkby, M. J. (1979). A physically based, variable contributing area model of basin hydrology. *Hydrological Sciences Bulletin*, 24(1):43–69, doi:10.1080/02626667909491834.

Bidel, Y., Zahzam, N., Blanchard, C., Bonnin, A., Cadoret, M., Bresson, A., Rouxel, D., and Lequentrec-Lalancette, M. F. (2018). Absolute marine gravimetry with matter-wave interferometry. *Nature Communications*, 9(1):627, doi:10.1038/s41467-018-03040-2.

Bonforte, A., Fanizza, G., Greco, F., Matera, A., and Sulpizio, R. (2017). Long-term dynamics across a volcanic rift: 21 years of microgravity and GPS observations on the southern flank of Mt. Etna volcano. *Journal of Volcanology and Geothermal Research*, 344:174–184, doi:10.1016/j.jvolgeores.2017.06.005.

Boy, J.-P. and Hinderer, J. (2006). Study of the seasonal gravity signal in superconducting gravimeter data. *Journal of Geodynamics*, 41(1-3):227–233, doi:10.1016/j.jog.2005.08.035.

Brunner, P. and Simmons, C. T. (2012). HydroGeoSphere: A Fully Integrated, Physically Based Hydrological Model. *Ground Water*, 50(2):170–176, doi:10.1111/j.1745-6584.2011.00882.x.

Carbone, D., Poland, M. P., Diament, M., and Greco, F. (2017). The added value of time-variable microgravimetry to the understanding of how volcanoes work. *Earth-Science Reviews*, 169(August 2016):146–179, doi:10.1016/j.earscirev.2017.04.014.

Cartwright, I., Morgenstern, U., Hofmann, H., and Gilfedder, B. (2020). Comparisons and uncertainties of recharge estimates in a temperate alpine catchment. *Journal of Hydrology*, 590:125558, doi:10.1016/j.jhydrol.2020.125558.

Clow, D., Schrott, L., Webb, R., Campbell, D., Torizzo, A., and Dornblaser, M. (2003). Ground Water Occurrence and Contributions to Streamflow in an Alpine Catchment, Colorado Front Range. *Ground Water*, 41(7):937–950, doi:10.1111/j.1745-6584.2003.tb02436.x.

Cochand, M., Christe, P., Ornstein, P., and Hunkeler, D. (2019). Groundwater Storage in High Alpine Catchments and Its Contribution to Streamflow. *Water Resources Research*, 55(4):2613–2630, doi:10.1029/2018WR022989.

Cowie, R. M., Knowles, J. F., Dailey, K. R., Williams, M. W., Mills, T. J., and Molotch, N. P. (2017). Sources of streamflow along a headwater catchment elevational gradient. *Journal of Hydrology*, 549:163–178, doi:10.1016/j.jhydrol.2017.03.044.

Creutzfeldt, B., Güntner, A., Klügel, T., and Wziontek, H. (2008). Simulating the influence of water storage changes on the superconducting gravimeter of the Geodetic Observatory Wettzell, Germany. *Geophysics*, 73(6), doi:10.1190/1.2992508.

Creutzfeldt, B., Güntner, A., Vorogushyn, S., and Merz, B. (2010). The benefits of gravimeter observations for modelling water storage changes at the field scale. *Hydrology and Earth System Sciences*, 14(9):1715–1730, doi:10.5194/hess-14-1715-2010.

Cutillo, P. A. and Bredehoeft, J. D. (2011). Estimating Aquifer Properties from the Water Level Response to Earth Tides. *Ground Water*, 49(4):600–610, doi:10.1111/j.1745-6584.2010.00778.x.

Eiken, O., Stenvold, T., Zumberge, M., Alnes, H., and Sasagawa, G. (2008). Gravimetric monitoring of gas production from the Troll field. *GEOPHYSICS*, 73(6):WA149–WA154, doi:10.1190/1.2978166.

El-Diasty, M. (2016). Groundwater storage change detection using micro-gravimetric technology. *Journal of Geophysics and Engineering*, 13(3):259–272, doi:10.1088/1742-2132/13/3/259.

GDAL/OGR Contributors (2020). GDAL/OGR: Geospatial Data Abstraction software Library.

Glas, R., Lautz, L., McKenzie, J., Mark, B., Baraer, M., Chavez, D., and Maharaj, L. (2018). A review of the current state of knowledge of proglacial hydrogeology in the Cordillera Blanca, Peru. *Wiley Interdisciplinary Reviews: Water*, 5(5):e1299, doi:10.1002/wat2.1299.

Harris, C. R., Millman, K. J., van der Walt, S. J., Gommers, R., Virtanen, P., Cournapeau, D., Wieser, E., Taylor, J., Berg, S., Smith, N. J., Kern, R., Picus, M., Hoyer, S., van Kerkwijk, M. H., Brett, M., Haldane, A., del Río, J. F., Wiebe, M., Peterson, P., Gérard-Marchant, P., Sheppard, K., Reddy, T., Weckesser, W., Abbasi, H., Gohlke, C., and Oliphant, T. E. (2020). Array programming with NumPy. *Nature*, 585(7825):357–362, doi:10.1038/s41586-020-2649-2.

Hayashi, M. (2020). Alpine Hydrogeology: The Critical Role of Groundwater in Sourcing the Headwaters of the World. *Groundwater*, 58(4):498–510, doi:10.1111/gwat.12965.

Hunter, J. D. (2007). Matplotlib: A 2D Graphics Environment. *Computing in Science & Engineering*, 9(3):90–95, doi:10.1109/MCSE.2007.55.

Immerzeel, W. W., Lutz, A. F., Andrade, M., Bahl, A., Biemans, H., Bolch, T., Hyde, S., Brumby, S., Davies, B. J., Elmore, A. C., Emmer, A., Feng, M., Fernández, A., Haritashya, U., Kargel, J. S., Koppes, M., Kraaijenbrink, P. D., Kulkarni, A. V., Mayewski, P. A., Nepal, S., Pacheco, P., Painter, T. H., Pellicciotti, F., Rajaram, H., Rupper, S., Sinisalo, A., Shrestha, A. B., Viviroli, D., Wada, Y., Xiao, C., Yao, T., and Baillie, J. E. (2020). Importance and vulnerability of the world's water towers. *Nature*, 577(7790):364–369, doi:10.1038/s41586-019-1822-y.

Jacob, T., Chery, J., Bayer, R., Le Moigne, N., Boy, J. P., Vernant, P., and Boudin, F. (2009). Time-lapse surface to depth gravity measurements on a karst system reveal the dominant role of the epikarst as a water storage entity. *Geophysical Journal International*, 177(2):347–360, doi:10.1111/j.1365-246X.2009.04118.x.

Jongmans, D. and Garambois, S. (2007). Geophysical investigation of landslides : a review. *Bulletin de la Société Géologique de France*, 178(2):101–112, doi:10.2113/gssgfbull.178.2.101.

Kudryavtsev, S. M. (2004). Improved harmonic development of the Earth tide-generating potential. *Journal of Geodesy*, 77(12):829–838, doi:10.1007/s00190-003-0361-2.

Leirião, S., He, X., Christiansen, L., Andersen, O. B., and Bauer-Gottwein, P. (2009). Calculation of the temporal gravity variation from spatially variable water storage change in soils and aquifers. *Journal of Hydrology*, 365(3-4):302–309, doi:10.1016/j.jhydrol.2008.11.040.

Longman, I. M. (1959). Formulas for computing the tidal accelerations due to the moon and the sun. *Journal of Geophysical Research*, 64(12):2351–2355, doi:10.1029/JZ064i012p02351.

Mari, S., Scapozza, C., and Pera, S. (2013). Prove di multitracciamento di ghiacciai rocciosi e ambienti periglaciali nel Vallon de Réchy (VS) e nella Valle di Sceru (TI). *Bollettino della Società ticinese di scienze naturali*, 101:13–20.

McClymont, A. F., Hayashi, M., Bentley, L. R., and Liard, J. (2012). Locating and characterising groundwater storage areas within an alpine watershed using time-lapse gravity, GPR and seismic refraction methods. *Hydrological Processes*, 26(12):1792–1804, doi:10.1002/hyp.9316.

Mouyen, M., Steer, P., Chang, K.-J., Le Moigne, N., Hwang, C., Hsieh, W.-C., Jeandet, L., Longuevergne, L., Cheng, C.-C., Boy, J.-P., and Masson, F. (2020). Quantifying sediment mass redistribution from joint time-lapse gravimetry and photogrammetry surveys. *Earth Surface Dynamics*, 8(2):555–577, doi:10.5194/esurf-8-555-2020.

Pool, D. R. and Eychaner, J. H. (1995). Measurements of Aquifer-Storage Change and Specific Yield Using Gravity Surveys. *Ground Water*, 33(3):425–432, doi:10.1111/j.1745-6584.1995.tb00299.x.

Ramillien, G., Famiglietti, J. S., and Wahr, J. (2008). Detection of Continental Hydrology and Glaciology Signals from GRACE: A Review. *Surveys in Geophysics*, 29(4-5):361–374, doi:10.1007/s10712-008-9048-9.

Rau, G. C. (2018). hydrogeoscience/pygtide: PyGTide v0.2 DOI:10.5281/zenodo.1346664.

Rau, G. C., Acworth, R. I., Halloran, L. J. S., Timms, W. A., and Cuthbert, M. O. (2018). Quantifying compressible groundwater storage by combining cross-hole seismic surveys and head response to atmospheric tides. *Journal of Geophysical Research: Earth Surface*, 123:1910–1930, doi:10.1029/2018JF004660.

Reitz, A., Krahenbuhl, R., and Li, Y. (2015). Feasibility of time-lapse gravity and gravity gradiometry monitoring for steam-assisted gravity drainage reservoirs. *GEOPHYSICS*, 80(2):WA99–WA111, doi:10.1190/geo2014-0217.1.

Scintrex (2018). *Autograv CG-6 Manual*. Scintrex Ltd., Concord, ON.

Seibert, J. E. and Brady, J. L. (2003). Potential ionospheric impacts on the Prudhoe Bay Alaska microgravity Waterflood Monitoring Survey. *GPS Solutions*, 6(4):271–272, doi:10.1007/s10291-002-0039-x.

Tapley, B. D., Bettadpur, S., Ries, J. C., Thompson, P. F., and Watkins, M. M. (2004). GRACE measurements of mass variability in the Earth system. *Science*, 305(5683):503–505, doi:10.1126/science.1099192.

Thomas, A. C., Reager, J. T., Famiglietti, J. S., and Rodell, M. (2014). A GRACE-based water storage deficit approach for hydrological drought characterization. *Geophysical Research Letters*, 41(5):1537–1545, doi:10.1002/2014GL059323.

Thompson, J. C. and Moore, R. D. (1996). Relations between topography and water table depth in a shallow forest soil. *Hydrological Processes*, 10(11):1513–1525, doi:10.1002/(sici)1099-1085(199611)10:11<1513::aid-hyp398>3.0.co;2-v.

Virtanen, P., Gommers, R., Oliphant, T. E., Haberland, M., Reddy, T., Cournapeau, D., Burovski, E., Peterson, P., Weckesser, W., Bright, J., van der Walt, S. J., Brett, M., Wilson, J., Millman, K. J., Mayorov, N., Nelson, A. R. J., Jones, E., Kern, R., Larson, E., Carey, C. J., Polat, I., Feng, Y., Moore, E. W., VanderPlas, J., Laxalde, D., Perktold, J., Cimrman, R., Henriksen, I., Quintero, E. A., Harris, C. R., Archibald, A. M., Ribeiro, A. H., Pedregosa, F., and van Mulbregt, P. (2020). SciPy 1.0: fundamental algorithms for scientific computing in Python. *Nature Methods*, 17(3):261–272, doi:10.1038/s41592-019-0686-2.

Viviroli, D., Dürr, H. H., Messerli, B., Meybeck, M., and Weingartner, R. (2007). Mountains of the world, water towers for humanity: Typology, mapping, and global significance. *Water Resources Research*, 43(7):1–13, doi:10.1029/2006WR005653.

Wenzel, H. G. (1996). The nanogal software: Earth tide data processing package ETERNA 3.30. *Bull. Inf. Marées Terrestres*, 124:9425–9439.